*Transactions of the 17th International Conference on Structural Mechanics in Reactor Technology (*SMiRT 17)
*Prague, Czech Republic, August 17 –22, 2003*
*Paper # C03-4*

# Prediction of Failure of Highly Irradiated Zircaloy Clad Tubes under Reactivity Initiated Accidents

Lars O. Jernkvist,
Quantum Technologies AB, Uppsala Science Park, SE-751 83 Uppsala, Sweden.

## ABSTRACT

This paper deals with failure of irradiated Zircaloy tubes under the heat-up stage of a reactivity initiated accident (RIA). More precisely, by use of a model for plastic strain localization and necking failure, we theoretically analyse the effects of local surface defects on clad ductility and survivability under RIA. The results show that even very shallow surface defects, *e.g.* arising from a non-uniform or partially spalled oxide layer, have a strong limiting effect on clad ductility. Moreover, in presence of surface defects, the ability of the clad tube to expand radially without necking failure is found to be extremely sensitive to the stress biaxiality ratio $\sigma_{zz}/\sigma_{\theta\theta}$, which is here assumed to be in the range from 0 to 1.

The results of our analysis are compared with clad ductility data available in literature, and their consequences for clad failure prediction under RIA are discussed. In particular, the results raise serious concerns regarding the applicability of failure criteria, which are based on clad strain energy density. These criteria do not capture the observed sensitivity to stress biaxiality on clad failure propensity.

**KEY WORDS:** RIA, Zircaloy, cladding, failure criterion, ductility, necking, plasticity, corrosion, strain energy, SED.

## INTRODUCTION

Light water reactor (LWR) fuel is subjected to several operational restrictions in order to secure clad tube integrity under various classes of anticipated operational transients and design basis accidents. A reactivity initiated accident, which is caused *e.g.* by an inadvertent control rod withdrawal, is among the most serious of these events. The worst scenarios for RIA are associated with complete failure of a control rod drive mechanism, leading to fast ejection of a control rod assembly in pressurized water reactors (PWR), or to a control rod drop in boiling water reactors (BWR). Although these scenarios are somewhat different in PWR and BWR, the fuel rods adjacent to the withdrawn control rod are in both reactor types subjected to a very fast (≈50 ms) local increase in power. This results in nearly adiabatic heating of the fuel pellets, which expand thermally and may cause fast straining of the surrounding Zircaloy clad tube through pellet-clad mechanical interaction (PCMI). At this early heat-up stage of the RIA, the clad tube material is still at a fairly low temperature (<650 K), and the fast straining imposed by the expanding fuel pellets may therefore cause a momentaneous and partially brittle mode of clad failure [1].

At a later stage, heat transferred from the pellets may bring the clad outer surface to such a high temperature that departure from nucleate boiling (DNB) occurs. If so, the clad material could remain at a temperature above 1000-1200 K for up to 10 s, until rewetting takes place [2]. This fairly long period at elevated temperature may lead to clad creep rupture, in cases where significant pressure differences exist across the clad wall. The clad rupture could either be in the form of outward ballooning or inward collapse, depending on whether the rod internal gas pressure exceeds the coolant pressure or *vice versa* [3]. In addition, a third mode of failure may occur during re-wetting of the overheated clad tube, since the abrupt quenching may cause brittle fracture and disruption of the clad material. This failure mode is imminent if the clad tube is severely oxidized.

Of the three different failure modes described above, PCMI-induced clad failures during the early heat-up stage of an RIA are pressumably the most restrictive for high-burnup fuel rods. Tests performed in pulse reactors under RIA-like conditions indicate that PCMI-induced failures are more likely to occur than DNB in high-burnup fuel [3], and these failures have therefore attracted much attention in research on fuel rod behaviour under RIA. This research has revealed that PCMI-induced failures start by inward crack propagation through the clad wall. It seems that crack initiation takes place easily, since post-test examinations generally reveal a large number of radially aligned incipient cracks through the clad outer oxide layer and the hydride- and oxygen rich layer of brittle material beneath the oxide [1,4]. Some of these incipient cracks then propagate through the remaining part of the clad wall in a ductile manner, exhibiting a characteristic fracture plane, which is oriented about 45° degrees to the main loading (hoop) direction. The ductile feature of the last part of the crack path is usually seen also in highly oxidized and embrittled clad materials.

The resulting perforations of the clad do not necessarily evolve into long axial splits of the tube [5,4], but if they do, large amounts of $UO_2$ material can be dispersed into the coolant. There is some dispute whether the primary defects grow axially through a fast and unstable propagation mechanism [6], or if the propagation takes place during cool down of the clad, *after* the actual transient. The latter hypothesis is supported by a delay in fission gas expulsion from failed rods, which has been observed in recent RIA tests [7].

Prevalent operational limits for RIA are formulated in terms of thresholds for peak fuel enthalpy, which must not be exceeded under certain postulated scenarios in order to preclude clad failure and fuel dispersal into the coolant. The enthalpy thresholds, upon which these acceptance criteria rely, were established from power pulse tests on fuel rods with low burnup in the late seventies and eighties. However, later tests on highly irradiated fuel rods have shown that clad tube failure may occur at fuel enthalpy levels, which are well below these thresholds [8]. This indicates that the propensity for clad failure increases with fuel burnup, probably due to closure of the pellet-clad gap, which aggravates PCMI, and the continuous deterioration of clad strength and ductility by radiation, oxidation and hydride formation.

From available results of recent pulse reactor tests, it is possible to draw some qualitative conclusions regarding PCMI-induced failures in high-burnup fuel rods under RIA [1,8]. Firstly, the large number of incipient cracks observed in the outer oxide layer and the subjacent rim of severely hydrided material indicates that these layers largely lack capacity to carry tensile loads. The survivability of the cladding will therefore depend on the thickness of the remaining inner layer of load-bearing material. The thickness of this layer is dictated by the clad oxidation, which in PWR is linked to the axial position along the fuel rod. However, there are also random fluctuations in the thickness of the inner load-bearing layer along the hoop direction, and the fact that one rod may survive, while a sibling rod fails in similar power pulse tests, can in part be explained by this variability. Secondly, since PCMI induces a displacement-controlled load on the clad tube, its survival will rely on the ductility of the clad inner layer, *i.e.* its ability to deform plastically without fracturing. The ductility depends on fast neutron dose, temperature, hydride distribution and stress state [9].

Computer simulations have been performed in parallel with recent RIA tests on high-burnup fuel rods, leading to a proposed new clad failure criterion, in which effects of oxidation and hydrogen-embrittlement are considered [10,11]. This criterion is not based on fuel enthalpy, but rather on the clad strain energy density (SED), which is calculated for a certain RIA by use of a transient analysis code. Failure/no failure predictions are obtained by comparing the calculated SED with a threshold value, which is experimentally determined from tensile- or burst tests on oxidized and hydrided clad materials. Hence, the assumption is that for a certain clad temperature, irradiation dose, hydrogen content and oxide layer thickness, the clad ductility and survivability are defined by a critical value of the strain energy density.

However, the clad failure criterion based on SED has so far not been particularly successful in retrodicting clad failures in performed RIA tests. This is probably due to the fact that the criterion is applied without consideration of localization effects, arising from *e.g.* a non-uniform oxide layer or hydride distribution. This paper presents a theoretical study on how local defects in the form of a partially spalled oxide layer, hydride blisters or fretting marks on the clad outer surface affect the clad ductility, and hence the survivability of highly irradiated fuel rods under RIA. The results of the analysis are compared with proposed SED-based clad failure thresholds.

## ANALYSIS OF LOCALIZED CLAD FAILURE

### Fundamental assumptions

Consider first an axisymmetric clad tube with uniform wall thickness, $t$. If $t/R << 1$, where $R$ is the tube average radius, the stress state in the clad material can be approximated by

$$\sigma_{\theta\theta}(r,\theta,z) = \sigma_o , \tag{1}$$

$$\sigma_{zz}(r,\theta,z) = \alpha\sigma_o , \tag{2}$$

$$\sigma_{rr} = \sigma_{r\theta} = \sigma_{rz} = \sigma_{z\theta} = 0 . \tag{3}$$

Here, $\sigma_{ij}$ is the Cauchy stress tensor, with $r,\theta,z$ denoting the radial, hoop and axial directions, and $\alpha = \sigma_{zz}/\sigma_{\theta\theta}$ is the stress biaxiality ratio. By setting $\sigma_o = pR/t$ and $\alpha = 1/2$, we obtain the familiar expressions for a closed-end thin-walled tube with inner overpressure $p$, which are the typical conditions for a clad burst test. Cases with $\alpha \neq 1/2$ correspond to modified axial loading, due to pellet-clad frictional contact. Henceforth, the stress biaxiality ratio $\alpha$ is treated as a parameter in our analysis. Since we are interested in loading conditions for which clad plastic deformation is dominant, we will neglect the contribution from clad elasticity to the total deformation. Moreover, we assume that the clad material is highly irradiated, and that the plastic deformation can be described by isotropic flow theory [12]. The components of plastic strain thus evolve according to the Lévy-Mises equations [13]

$$\dot{\varepsilon}_{ij} = \lambda(\sigma_e,\varepsilon_e)s_{ij} , \tag{4}$$

where $\varepsilon_{ij}$ are the plastic strain rates and $s_{ij}$ are the deviatoric stresses, defined by

$$s_{ij} = \sigma_{ij} - \frac{\sigma_{kk}}{3}\delta_{ij} . \tag{5}$$

Here, $\delta_{ij}$ is the Krönecker delta, and repeated indices imply summation over $r$, $\theta$ and $z$. The scalar $\lambda$ in eq. (4) is a non-negative function of the von Mises effective stress and the effective plastic strain, $\varepsilon_e$, which are defined through

$$\sigma_e = \sqrt{\frac{3}{2} s_{ij} s_{ij}} \ , \tag{6}$$

$$\dot{\varepsilon}_e = \sqrt{\frac{2}{3} \dot{\varepsilon}_{ij} \dot{\varepsilon}_{ij}} = \lambda \sqrt{\frac{2}{3} s_{ij} s_{ij}} = \frac{2\lambda}{3} \sigma_e \, . \tag{7}$$

Under the stress state defined in eqs. (1)-(3), we have

$$\sigma_e = \sigma_o \sqrt{1 - \alpha + \alpha^2} \ . \tag{8}$$

**Effect of clad surface defects**

Consider a deviation from the perfect axisymmetric tube geometry in the form of a long shallow groove, which extends along the tube outer surface, as illustrated in figure 1. The surface defect could be a fretting mark, caused by clad/spacer grid contact, but it could also result from non-uniform waterside corrosion. In the latter case, the shaded area represents a spalled or cracked oxide layer or a cracked hydride blister, without ability to carry tensile loads. The thickness of the remaining load-bearing part of the clad wall is denoted by $g$.

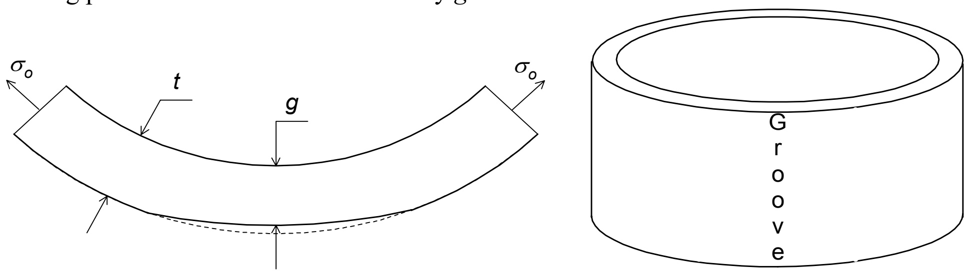


Fig 1. A clad surface defect in the form of a long, shallow groove is considered in analyses.

Since the groove is assumed to be shallow, *i.e.* its width in the hoop direction is larger than the clad thickness, shear stresses as well as radial gradients in stress and strain across the clad thickness may be neglected. Hence, the stresses at the groove can be written

$$\sigma^g_{\theta\theta}(r,\theta,z) = \sigma_o \, t/g \, , \tag{9}$$

$$\sigma^g_{zz}(r,\theta,z) = \beta \sigma^g_{\theta\theta} \, , \tag{10}$$

$$\sigma^g_{rr} = \sigma^g_{r\theta} = \sigma^g_{rz} = \sigma^g_{z\theta} = 0 \, , \tag{11}$$

where superscript $g$ alludes to the local conditions at the groove. Equation (9) is obtained from the requirement on equilibrium between the tapered cross-section at the groove and the surrounding material, in which the stress state is defined by eqs. (1)-(3). The parameter $\beta$ in eq. (10) defines the local stress biaxiality at the groove. It is generally not equal to $\alpha$, and must be determined from a requirement on compatible axial deformation between the groove ( $\varepsilon^g_{zz}$ ) and the surrounding material ( $\varepsilon_{zz}$ )

$$\dot{\varepsilon}^g_{zz} = \dot{\varepsilon}_{zz} \, . \tag{12}$$

From eqs. (9)-(11), we find the von Mises effective stress at the groove

$$\sigma^g_e = \frac{\sigma_o t}{g} \sqrt{1 - \beta + \beta^2} \ . \tag{13}$$

By combining eqs. (8), (9) and (13) we obtain

$$\frac{\sigma^g_e \, g}{\sigma_e \, t} = \sqrt{\frac{1 - \beta + \beta^2}{1 - \alpha + \alpha^2}} \ . \tag{14}$$

The compatibility condition in eq. (12) can be expressed in terms of effective plastic strain rates by applying eqs. (4), (5) and (7) to the stress states defined in eqs. (1)-(3) and eqs. (9)-(11), respectively

$$\frac{\dot{\varepsilon}_e^g \left( 2\beta - 1 \right)}{\dot{\varepsilon}_e \left( 2\alpha - 1 \right)} = \sqrt{\frac{1 - \beta + \beta^2}{1 - \alpha + \alpha^2}} \quad . \tag{15}$$

Finally, by combining eqs. (14) and (15), we find

$$\beta = \frac{1}{2} \left[ 1 + \left( 2\alpha - 1 \right) \frac{\sigma_e^g \, \dot{\varepsilon}_e \, g}{\sigma_e \, \dot{\varepsilon}_e^g \, t} \right] . \tag{16}$$

It is interesting to note that for $\alpha = 1/2$, eq. (16) yields $\beta = 1/2$. This particular choice of $\alpha$ thus results in plane strain plastic deformation, both at the groove and in the surrounding material; *i.e.* $\varepsilon_{zz}^g = \varepsilon_{zz} = 0$ .

**Constitutive relation**

In order to determine the evolution of plastic deformation at the groove and in the surrounding material, we use a material model, which considers both strain- and strain rate hardening

$$\sigma_e = \sigma_y \left( \frac{\varepsilon_e}{\varepsilon_o} \right)^n \left( \frac{\dot{\varepsilon}_e}{\dot{\varepsilon}_o} \right)^m , \tag{17}$$

where $\varepsilon_o = 0.002$ and $\dot{\varepsilon}_o = 8.33 \cdot 10^{-5}$ $s^{-1}$ are constants used for normalization [14]. The yield stress $\sigma_y$ and the hardening exponents $n$ and $m$ are material properties, which depend on temperature and fast neutron fluence. Simple expressions for these parameters were fitted to literature data from axial tensile tests and burst tests on clad tubes of recrystallized Zircaloy-2, covering temperatures $T$ from 293 to 673 K, fast neutron fluences $\phi$ (>1 MeV) from 0 to $8.5 \times 10^{25}$ neutrons per $m^2$ and effective strain rates from $8.33 \times 10^{-5}$ to $7.5 \times 10^{-3}$ $s^{-1}$. The yield stress can be expressed by

$$\sigma_y = \overline{\sigma} \left( 1 + A \left( \frac{\phi}{10^{24}} \right)^l \right) , \tag{18}$$

where $\overline{\sigma} = 6.578 \cdot 10^8 (1 - 1.686 \cdot 10^{-3} T + 7.748 \cdot 10^{-7} T^2)$ Pa, $A = 4.238 \cdot 10^{-1} + 1.618 \cdot 10^{-3} T$ and $l = 3.551 \cdot 10^{-2} + 1.926 \cdot 10^{-4} T$ . The strain hardening exponent is given by

$$n = 0.06 \left( 1 + 1.244 \cdot 10^{-3} T \right) F(\phi) , \tag{19}$$

where $F(\phi) = 1 - 1.239 \cdot 10^{-27} \phi + 4.169 \cdot 10^{-53} \phi^2 - 9.458 \cdot 10^{-1} \tanh(4.461 \cdot 10^{-24} \phi)$ . In all these expressions, $T$ is in Kelvin and $\phi$ is in neutrons per $m^2$. Finally, the strain rate hardening exponent is assumed to be constant, $m = 0.02$.

**Evolution of clad thickness**

The clad thickness changes as a result of plastic deformation. By denoting the original clad thicknesses $t_o$ and $g_o$, the definition of true (logarithmic) strain in the radial direction yields [13]

$$t = t_o \, e^{\varepsilon_{rr}} , \tag{20}$$

$$g = g_o \, e^{\varepsilon_{rr}^g} , \tag{21}$$

where the accumulated radial strains can be calculated from

$$\dot{\varepsilon}_{rr} = - \frac{\dot{\varepsilon}_e \left( 1 + \alpha \right)}{2 \sqrt{1 - \alpha + \alpha^2}} , \tag{22}$$

$$\dot{\varepsilon}_{rr}^g = - \frac{\dot{\varepsilon}_e^g \left( 1 + \beta \right)}{2 \sqrt{1 - \beta + \beta^2}} . \tag{23}$$

These expressions are found by once again applying eqs. (4), (5) and (7) to the stress states defined in eqs. (1)-(3) and eqs. (9)-(11), respectively. In our analysis, we assume that $g_o < t_o$, which results in necking, *i.e.* failure through a gradually accelerating localization of plastic deformation to the groove. As will be shown in the sequel, this localization is very sensitive to the initial depth of the clad surface defect, which for convenience is denoted by $f$

$$f = \left( 1 - \frac{g_o}{t_o} \right) . \tag{24}$$

Here, we are interested in shallow grooves of moderate depth, *i.e.* cases where $f$ ranges from 0.0 to about 0.1.

**Final system of equations**

By assuming that the constitutive relation in eq. (17) applies to the material at both the groove and its surroundings, and that the temperature and fast neutron fluence are uniform along the clad hoop direction, we find from eqs. (14) and (17)

$$\dot{\varepsilon}_e^g \;=\; \dot{\varepsilon}_e \left[ \frac{t}{g} \sqrt{\frac{1 - \beta + \beta^2}{1 - \alpha + \alpha^2}} \left( \frac{\varepsilon_e}{\varepsilon_e^g} \right)^n \right]^{1/m} . \tag{25}$$

Departing from the above equation, the time evolution for stress, strain and clad thickness both outside and in the groove can be calculated, provided that the stress biaxiality ratio $\alpha$ and the uniform effective strain rate $\dot{\varepsilon}_e$ are given. For the particular choice of $\alpha = 1/2$, it is possible to find closed-form analytical solutions to all parameters [15], but for other values of $\alpha$, eq. (25) must be numerically integrated in tandem with eqs. (16), (20) and (21).

**RESULTS**

Typical solutions to the derived systems of equations, (16), (20), (21) and (25), are shown in figure 2, where the local hoop strain at the groove $\varepsilon^{s}_{\theta\theta}$ is plotted as a function of the uniform hoop strain $\varepsilon_{\theta\theta}$, *i.e.* the strain outside the groove. Results are shown for three different initial depths of the defect. In all three cases, the stress biaxiality ratio $\alpha$ was 1/2, the effective strain rate was $1\times10^{-3}$ $s^{-1}$ and the clad temperature and fast neutron fluence were 600 K and $1\times10^{25}$ neutrons per $m^2$.

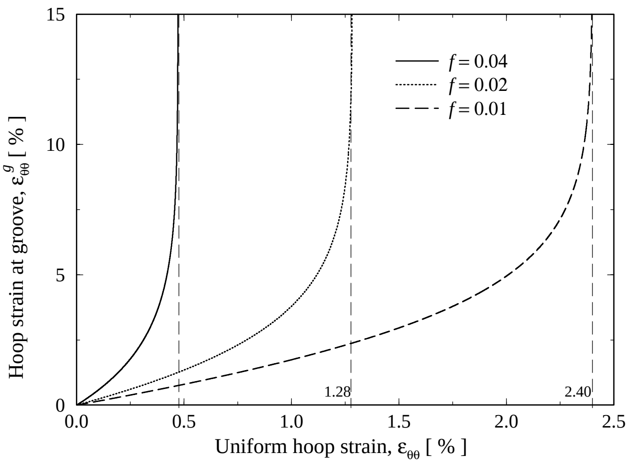


Fig 2. Clad strain localization behaviour (necking) as a function of relative depth of the defect, *f*. Here, the assumed stress biaxiality ratio $\alpha$ is 1/2.

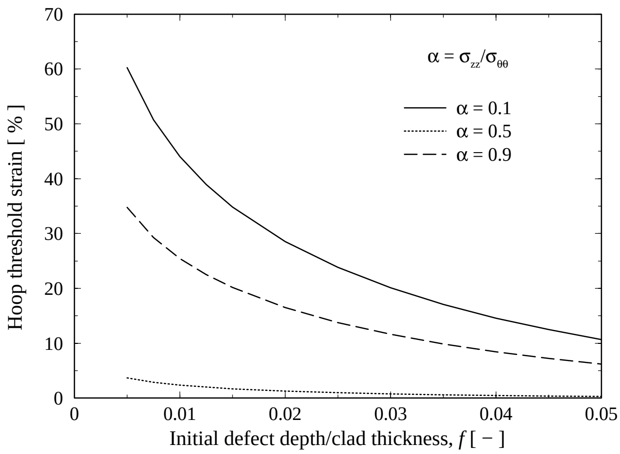


Fig 3. Calculated sensitivity of clad hoop threshold strain to stress biaxiality and relative defect depth.

Clearly, as an effect of strain localization, the hoop strain at the groove approaches infinity at very moderate values of uniform hoop strain, 0.47, 1.28 and 2.40%, depending on the initial depth of the groove. These values should be interpreted as “threshold strains”, at which the clad inevitably fails by necking at the groove. The threshold strain is not only dependent on the initial defect depth, but also on the stress biaxiality ratio $\alpha = \sigma_{zz}/\sigma_{\theta\theta}$. This is illustrated in figure 3, which shows that the hoop threshold strain is particularly low for $\alpha = 1/2$. This stress state is the one obtained in clad burst tests, and for isotropic materials, it results in plane strain plastic deformation in the tube axial direction.

As shown in figure 4, the calculated hoop threshold strain has a minimum for $\alpha = 1/2$, irrespective of the initial depth of the clad surface defect. The clad temperature and fast neutron fluence assumed in figures 3 and 4 are the same as for figure 2. Figure 5 shows the influence of clad temperature and fast neutron fluence on the hoop threshold strain for the particular case of $f = 0.02$ and $\alpha = 1/2$. The most important material parameter with respect to the necking behaviour is the strain hardening exponent $n$. In the material model applied here, $n$ depends on both temperature and fast neutron fluence; see eq. (19).

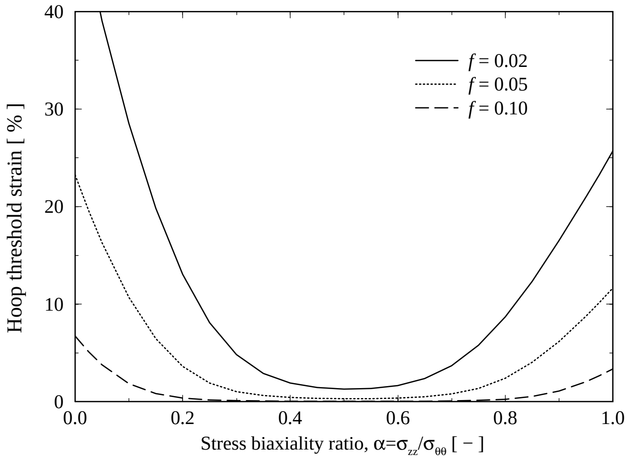


Fig 4. Calculated influence of stress biaxiality on hoop threshold strain.

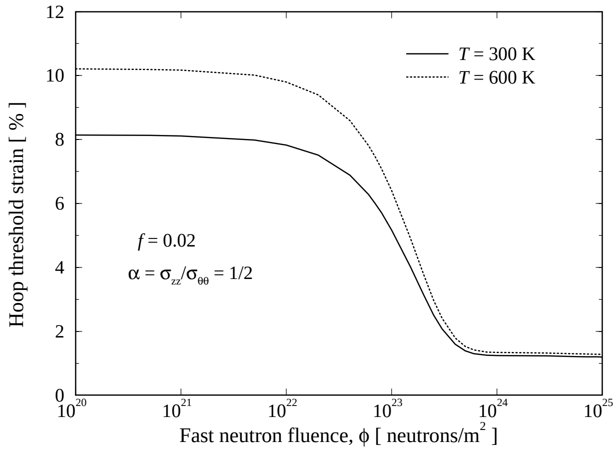


Fig 5. Calculated influence of clad temperature and fast neutron fluence on hoop threshold strain.

## DISCUSSION

### Comparison with Zircaloy ductility data

The results presented in the foregoing section indicate that failure of highly irradiated clad tubes through necking may occur at low uniform strain, also for very shallow surface defects. Moreover, the results show that the hoop threshold strain, *i.e.* the uniform hoop strain at which necking failure occurs, is extremely sensitive to the stress biaxiality ratio. These results, obtained from our purely theoretical model, should be discussed in light of experimental data.

Firstly, we note that the as-fabricated wall thickness of commercial clad tubes typically deviates by ± 2 to 3% from its nominal value around the perimeter of a given cross section, and that it is therefore motivated to assume that $f \approx 0.02$ also for unirradiated clad tubes, which are seemingly free of surface defects. With this assumption, figure 5 reveals that the uniform hoop strain at clad failure should decrease from about 10% to 1.3% as a result of irradiation, when burst testing ($\alpha$ = 1/2) of uniformly oxidized and defect free clad tubes at 600 K is considered. These results are in fair agreement with several experimental investigations, both for Zircaloy-2 and Zircaloy-4 materials [9,16]. The main reason for the predicted decrease in ductility with irradiation is the loss of strain hardening.

The hoop threshold strain, *i.e.* the uniform hoop strain at which necking failure occures, is according to figure 3 dependent on the relative depth of the surface defect. Pettersson *et al.* early recognized this influence of surface defects on the ductility of irradiated clad tubes by performing burst tests on irradiated Zircaloy-2 specimens with machined defects, which were 1.5 mm long and ranged in depth from 7 to 28% of the clad thickness [16]. Although our model does not treat the sharp and finite-length surface defects used in their test, it still captures the general trend in reported failure strains. What is even more interesting with figure 3 is the predicted sensitivity of the hoop threshold strain to the stress biaxiality ratio $\alpha = \sigma_{zz} / \sigma_{\theta\theta}$. This sensitivity is further explored in figure 4, which shows that a minimum seems to exist for $\alpha$ = 1/2, *i.e.* the stress state typical for clad burst tests. A sharp decrease in hoop threshold strain (ductility) has been observed experimentally for both irradiated and unirradiated Zircaloy, when changing the stress state from $\alpha$ = 0 to $\alpha$ = 1/2 [9,17,18]. However, the predicted gain in ductility, when going from $\alpha$ = 1/2 to $\alpha$ = 1 in figure 4, is in conflict with the experimental results for unirradiated materials presented in [17] and [18]. This prediction is therefore probably an artefact, resulting from the simplistic assumption of isotropic strain hardening in our model.

### Consequences for clad failure prediction under RIA

The ability of the clad tube to deform plastically in the hoop direction without necking failure is thus strongly affected by the clad stress state. As a consequence, ductility data obtained from uniaxial tensile tests, either in the clad axial or hoop direction, are rarely meaningful in predictions of PCMI-induced RIA-failures, where biaxial stress states prevail. This has been realized by some investigators, who have designed notched ring tensile specimens, in which a stress state close to $\alpha = \sigma_{zz}/\sigma_{\theta\theta}$ = 1/2 is obtained also under uniaxial loading [19,20]. Another consequence of the observed sensitivity to stress biaxiality is that any computer code intended to predict clad failure under RIA must be able to accurately model the PCMI-induced biaxial loading of the clad tube. In fresh fuel, this loading stems solely from thermal expansion of the solid fuel pellets. In high-burnup fuel, however, there is also a contribution from the thermally induced expansion of gaseous fission products, which are accumulated in pellet pores and intergranular bubbles. This contribution to the mechanical loading is difficult to model in computer codes, since it is strongly linked to the high-burnup redistribution of accumulated fission gases in the pellet rim zone [21].

Another difficulty in modelling PCMI-induced loads in high-burnup fuel is due to the closure of the pellet-clad gap and the formation of a bonding interface layer [6]. If such a layer exists at onset of an RIA, the axial friction forces transferred to the clad from the expanding fuel pellets are significantly higher than in regions where the gap is open prior to the transient. Hence, the stress biaxiality in the clad tube is dictated by the pellet-clad gap conditions at onset of RIA, and may therefore vary significantly with axial position along the fuel rod. To this end, it should be noticed that the measurements of average clad axial elongation, which are performed either under or after pulse reactor RIA tests, do not provide sufficient information to establish this axial variation in stress biaxiality.

### Comparison with SED-based failure thresholds

Finally, it could be interesting to compare our necking failure model with two existing RIA failure thresholds, in which the clad strain energy density (SED) is used as a critical parameter for failure. By use of the notation applied in earlier sections, the strain energy density in a body with predominantly plastic deformation can be approximated through

$$\mathrm{SED} = \frac{\sigma_y^2}{2E} + \int_{\varepsilon_0}^{\varepsilon_e} \sigma_e \, d\varepsilon_e' , \tag{26}$$

where $E$ is the Zircaloy clad elastic modulus, which is approximately 90 GPa for the material and operating conditions considered here [22]. The two right-hand side terms represent contributions from elastic and plastic deformation, respectively. Failure predictions are obtained by comparing the calculated SED under an RIA with a threshold value, which is experimentally determined from mechanical tests on oxidized and irradiated clad materials.

Rashid and co-workers have proposed a correlation for this failure threshold, based on data from clad burst tests and uniaxial tensile tests in both the axial and hoop directions [11]. Recently, del Barrio and Herranz derived a similar correlation from uniaxial hoop tensile tests [10]. These correlations are plotted with respect to relative clad oxide layer thickness in figure 6. The considered case is for $T$ = 600 K, $\dot{\varepsilon}_e = 1\times10^{-3}$ s$^{-1}$, $\alpha = \sigma_{zz}/\sigma_{\theta\theta} = 0.15$ and $\phi = 1\times10^{25}$ neutrons per m$^2$. Figure 6 also contains predictions from our necking failure model. These curves, denoted I and II, show the calculated uniform SED, *i.e.* the SED outside the groove, at which necking failure takes place. Case I represents a partially spalled clad oxide layer, for which the initial defect depth is given by $f$ = 0.02 + oxide/clad thickness. Hence, we assume that there is a 2% as-fabricated variation in clad wall thickness, which is then aggravated by oxide spalling. In case II, we instead assume that the oxide layer thickness varies by ±20% along the clad perimeter, which means that the initial clad defect depth is assumed to be $f$ = 0.02 + 0.2×oxide/clad thickness.

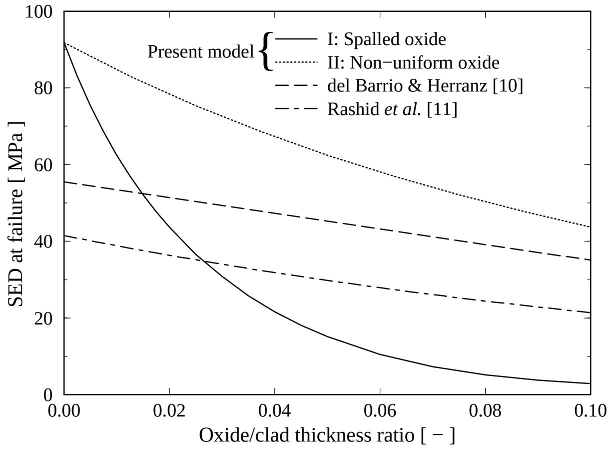


Fig 6. Comparison of our necking failure model with proposed SED-based failure thresholds [10,11]. A fixed stress biaxiality ratio ($\alpha$ = 0.15) is assumed.

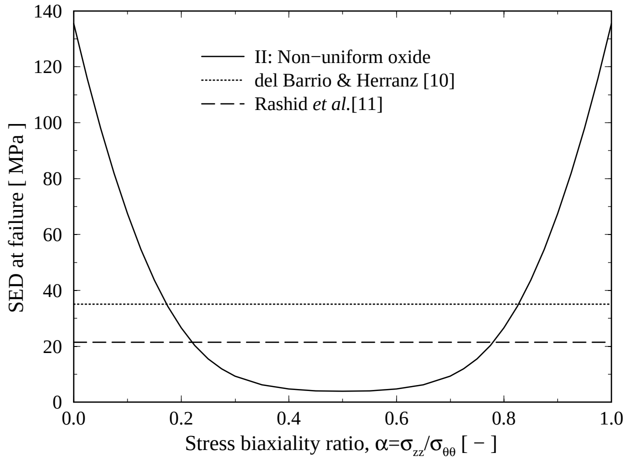


Fig 7. Influence of stress biaxiality on predicted SED at failure for case II. The proposed failure thresholds in [10,11] are independent of $\alpha$.

Evidently, our localization model predicts a more pronounced influence of the oxide thickness than that given by the empirical correlations in [10,11]. For case I (spalled oxide), the calculated SED at failure drops very fast with increasing oxide thickness, whereas case II (non-uniform oxide) follows about the same trend as the empirical correlations. This is not surprising, since the correlations are derived from tests on clad tubes with non-spalled oxide layers.

An *ad hoc* assumption behind the use of SED in a clad failure criterion is that the SED at failure is an inherent material property, which is independent of the clad stress state. Hence, clad failure should occur at the same threshold SED, irrespective of the stress biaxiality ratio, $\alpha = \sigma_{zz}/\sigma_{\theta\theta}$. This assumption is tested by use of our necking failure model in figure 7, in which SED at failure is plotted for a fixed oxide/clad thickness ratio of 0.10. The clad temperature, strain rate and irradiation dose is the same as for figure 6, but here, we have only considered case II; *i.e.* the case of a non-uniform oxide layer, whose thickness varies by ±20% along the clad perimeter.

In contrast to the assumption behind the empirical correlations, our necking failure model predicts that SED at failure is highly dependent on the stress biaxiality ratio. If clad failure under the initial heat-up stage of an RIA takes place by localized plastic deformation, as assumed in our model, the applicability of the SED-based failure thresholds proposed in [10] and [11] must therefore be questioned. They could possibly be used, if the stress biaxiality is introduced as a parameter in the correlations for SED at failure. However, the presently assumed independence of SED at failure with respect to stress state is not correct. This follows not only from the analysis presented here, but also from the way SED at failure is determined from uniaxial tensile tests in [10] and [11].

**CONCLUSIONS**

The influence of spalled oxide, hydride blisters, fretting marks and other surface defects on clad ductility was theoretically studied by a simple isotropic model for plastic strain localization and necking failure. The results show that even very shallow surface defects may have a strong limiting effect on the ducility of irradiated clad materials. Moreover, in presence of surface defects, the ability of the clad tube to expand radially without necking failure is found to be extremely sensitive to the stress biaxiality ratio $\sigma_{zz}/\sigma_{\theta\theta}$, which is here assumed to be in the range from 0 to 1. These findings are well in line with experimental data on clad ductility and defect sensitivity in literature, and their consequences for clad failure prediction under the heat-up stage of reactivity initiated accidents were discussed.

To this end, our necking failure model was compared with proposed RIA failure criteria, in which the clad strain energy density is used as a critical parameter for failure. The comparison raises concerns regarding the applicability of these criteria, which do not capture the influence of stress biaxiality on clad ductility and propensity for failure.

Finally, it should be noticed that the presented model treats strain localization and necking failure solely as results of variations in clad wall thickness along the tube periemeter. However, similar variations in clad wall temperature and material properties could be equally important for localization effects. This comment has particular relevance to clad tubes with partially spalled oxide, for which the ductility is reduced by a combination of local drop in temperature, local hydride precipitation and geometrical localization effects at the spalled spots.

**ACKNOWLEDGEMENT**

Financial support from the Swedish Nuclear Power Inspectorate (SKI) for part of this work is gratefully acknowledged.

**REFERENCES**

1. Chung, H.M. and Kassner, T.F., Cladding metallurgy and fracture behaviour during reactivity-initiated accidents at high burnup, *Nucl. Engnrg. Design*, Vol. 186, 1998, pp. 411-427.
2. Fuketa, Sasajima and Sugiyama, Behavior of high-burnup PWR fuels with low-tin Zr-4 cladding under reactivity initiated accident conditions, *Nucl. Techn*. Vol. 133, 2001, pp 50-62.
3. Ishijima and Nakamura, Transient elongation of a fresh fuel rod under reactivity initiated accident conditions, *Nucl. Sci. Techn*. Vol. 33(3), 1996, pp. 229-238.
4. Daum, R.S., Majumdar, S., Bates, D.W., Motta, A.T., Koss, D.A. and Billone, M.C. On the embrittlement of Zircaloy-4 under RIA-relevant conditions, *Zirc. Nucl. Ind.: 13th Int. Symp*. ASTM STP-1423, 2002, pp. 702-719.
5. Montgomery, R.O., Rashid, Y.R., Ozer, O. and Yang, R.L., Review and analysis of RIA-simulation experiments on intermediate- and high-burnup test rods, *Proc. Int. Topical Mtg. on LWR Fuel Performance*, 1997, pp. 711-720.
6. Chung, H.M., Fundamental metallurgical aspects of axial splitting in Zircaloy cladding, *Proc. Int. Topical Mtg. on LWR Fuel Performance*, April 10-13, 2000, Park City, Utah, U.S.A.
7. Waeckel, N., Bernaudat, C. and Salles, B., EDF proposed safety domain for rod ejection accidents in a PWR, *Proc. Int. Topical Mtg. on LWR Fuel Performance*, April 10-13, 2000, Park City, Utah, U.S.A.
8. Meyer, R.O., McCardell, R.K. and Scott, H.H., A regulatory assessment of test data for reactivity accidents, *Proc. Int. Topical Mtg. on LWR Fuel Performance*, 1997, pp. 729-744.
9. Garde, A.M., Smith, G.P. and Pirek, R.C., Effects of hydride precipitate localization and neutron fluence on the ductility of irradiated Zircaloy-4, *Zirc. Nucl. Ind.: 11th Int. Symp*. ASTM STP-1295, 1996, pp. 407-430.
10. del Barrio, M.T. and Herranz, L.E., Predictive methodology of a cladding failure criterion based on PROMETRA database: application to CABRI-CIP01 experiment, *Enlarged Halden programme group meeting*, September 8-13, 2002, Gol, Norway. Halden project report HPR-359, Vol. 2, paper 32.
11. Rashid, Y.R., Montgomery, R.O., Lyon, W.F. and Yang, R., A cladding failure model for fuel rods subjected to operational and accident transients, *Paper 3.5, IAEA Technical Committee Meeting on Nuclear Fuel Behaviour Modelling at High Burnup and Its Experimental Support*, June 18-23, 2000, Windermere, UK.
12. Nakatsuka, M. and Nagai, M., Reduction of plastic anisotropy of Zircaloy cladding by neutron irradiation, I: Yield loci obtained from Knoop hardness, *J. Nucl. Sci. and Technology*, Vol. 24(10), 1987, pp. 832-838.
13. Hill, R., *The mathematical theory of plasticity*, Oxford University Press, Oxford, UK, 1950.
14. ASTM E8-01, *Standard test methods for tension testing of metallic materials*, ASTM, 2001.
15. Chan, K.S., Koss, D.A. and Ghosh, A.K., Localized necking of sheet at negative minor strains, *Metall. Trans. A*, Vol. 15A, 1984, pp. 323-329.
16. Pettersson, K., Vesterlund, G. and Andersson, T., Effect of irradiation on the strength, ductility and defect sensitivity of fully recrystallized Zircaloy tube, *Zirc. Nucl. Ind.: 4th Int. Conf*. ASTM STP 681, 1979, pp. 155-173.
17. Yunchang, F. and Koss, D.A., The influence of multiaxial states of stress on the hydrogen embrittlement of zirconium alloy sheet, *Metallurgical Trans. A*, Vol. 16A, 1985, pp. 675-681.
18. Andersson, T. and Wilson, A., Ductility of Zircaloy canning tubes in relation to stress ratio in biaxial testing, *Zirconium in the Nuclear Industry: 4th Int. Conf*. ASTM STP 681, 1979, pp. 60-71.
19. Wisner, S.B. and Adamson, R.B., Combined effects of radiation damage and hydrides on the ductility of Zircaloy-2, *Nucl. Engnrg. Design*, Vol. 185, 1998, pp 33-49.
20. Link, T.M., Koss, D.A. and Motta, A.T., Failure of Zircaloy cladding under transverse plane-strain deformation, *Nucl. Engnrg. Design*, Vol. 186, 1998, pp 379-394.
21. Lemoine, F., High burnup fuel behaviour related to fission gas effects under reactivity initiated accidents (RIA) conditions, *J. Nucl. Mat*. Vol. 248, 1997, pp 238-248.
22. Hagrman, D.L., Reymann, G.A. and Mason, R.E., *MATPRO-Version 11 (revision 2): A handbook of materials properties for use in the analysis of light water reactor fuel rod behavior*, U.S. Nuclear Regulatory Commission report NUREG/CR-0497, August 1981.